J|A|C|S
ARTICLES
Published on Web 09/22/2006

Dramatic Acceleration of Olefin Epoxidation in Fluorinated Alcohols: Activation of Hydrogen Peroxide by Multiple H-Bond Networks

Albrecht Berkessel* and Jens A. Adrio

Contribution from the Institut für Organische Chemie, Universität zu Köln, Greinstrasse 4, D-50939 Köln, Germany

Received March 23, 2006; E-mail: berkessel@uni-koeln.de

Abstract: In 1,1,1,3,3,3-hexafluoro-2-propanol (HFIP) as solvent, the epoxidation of olefins by hydrogen peroxide is accelerated up to ca. 100 000-fold (relative to that in 1,4-dioxane as solvent). The mechanistic basis of this effect was investigated kinetically and theoretically. The kinetics of the epoxidation of *Z*-cyclooctene provided evidence that higher-order solvent aggregates (rate order in HFIP ca. 3) are responsible for the rate acceleration. Activation parameters ($\Delta S^{\ddagger} = -39$ cal/mol·K) indicated a highly ordered transition state in the rate-determining step. In line with these findings, DFT simulations revealed a pronounced decrease of the activation barrier for oxygen transfer from H_2O_2 to ethene with increasing number of (specifically) coordinated HFIP molecules. The oxygen transfer was unambiguously identified as a polar concerted process. Simulations (combined DFT and MP2) of the epoxidation of *Z*-butene were in excellent agreement with the experimental data obtained in the epoxidation of *Z*-cyclooctene (activation enthalpy, entropy, and kinetic rate order in HFIP of 3), supporting the validity of our mechanistic model.

Introduction

For the epoxidation of olefins, aqueous hydrogen peroxide is a most attractive terminal oxidant: it is readily available and safe to handle, has a high content of active oxygen, and produces water as the only side product. Remarkable advances have been made with regard to transition metal catalysts for the activation of H_2O_2.[1] On the other hand, fluorinated alcohols such as 2,2,2-trifluoroethanol (TFE) and 1,1,1,3,3,3-hexafluoro-2-propanol (HFIP) as solvents have been reported to remarkably accelerate oxidation processes with hydrogen peroxide,[2] occasionally even by opening entirely new reaction channels.[3] Of particular interest is the observation that these solvents are capable of activating H_2O_2 for the epoxidation of electron-rich olefins, even in the absence of an additional catalyst (eq 1).[4] Thus, olefin epoxidation in fluoroalcohols is the prototype of a purely organocatalytic epoxidation process with H_2O_2. Compared to metal catalysis, oxygen transfer must be effected by an entirely new mode of activation.

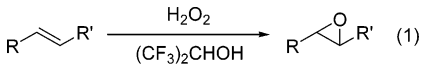

(1)

An initial quantum-chemical investigation of the mechanism of olefin epoxidation in fluoroalcohols was carried out by Shaik et al.[5] The authors proposed two major contributions of the fluoroalcohol to the polar, concerted oxygen-transfer reaction (Figure 1): the fluoroalcohol activates the oxidant (i) by acting as a strong hydrogen bond donor and (ii) by juxtapositioning of positive and negative partial charges within the transition states (TSs). Thus, the fluorinated alcohol forms a complementary charge template, causing significant electrostatic stabilization.

In their theoretical study, Shaik et al. considered a *monomolecular* mode of activation by the fluorinated alcohols for all reaction pathways analyzed.[5] On the other hand, we have recently reported experimental evidence that *higher-order aggregates* of fluorinated alcohols are decisive for the catalytic activity of this type of solvent, and in particular for HFIP.[6,7] We herein draw a detailed picture of the reaction mechanism based on additional kinetic data as well as extensive quantum-chemical simulations of reaction pathways encompassing higher-order HFIP coordination in the oxygen-transfer step.

Experimental Results

Although the activation of hydrogen peroxide for olefin epoxidation by fluorinated alcohols is well documented in the

(1) Adolfsson, H. In *Modern Oxidation Methods*; Bäckvall, J.-E., Ed.; Wiley-VCH: Weinheim, 2004.
(2) Vliet, M. C. A. v.; Arends, I. W. C. E.; Sheldon, R. A. *Tetrahedron Lett.* **1999**, *40*, 5239−5242. Ravikumar, K. S.; Bégué, J.-P.; Bonnet-Delpon, D. *Tetrahedron Lett.* **1998**, *39*, 3141−3144. Ravikumar, K. S.; Barbier, F.; Bégué, J.-P.; Bonnet-Delpon, D. *J. Fluorine Chem.* **1999**, *95*, 123−125. Vliet, M. C. A. v.; Arends, I. W. C. E.; Sheldon, R. A. *J. Chem. Soc., Perkin Trans. 1* **2000**, 377−380. Vliet, M. C. A. v.; Arends, I. W. C. E.; Sheldon, R. A. *Chem. Commun.* **1999**, 821−822. Legros, J.; Crousse, B.; Bonnet-Delpon, D.; Bégué, J.-P. *Tetrahedron* **2002**, *58*, 3993−3998. Legros, J.; Crousse, B.; Bonnet-Delpon, D.; Bégué, J.-P. *Eur. J. Org. Chem.* **2002**, 3290−3293. Berkessel, A.; Andreae, M. R. M. *Tetrahedron Lett.* **2001**, *42*, 2293−2295.
(3) Berkessel, A.; Andreae, M. R. M.; Schmickler, H.; Lex, J. *Angew. Chem., Int. Ed.* **2002**, *41*, 4481−4484.
(4) Neimann, K.; Neumann, R. *Org. Lett.* **2000**, *2*, 2861−2863. Vliet, M. C. A. v.; Arends, I. W. C. E.; Sheldon, R. A. *Synlett* **2001**, 248−250.
(5) de Visser, S. P.; Kaneti, J.; Neumann, R.; Shaik, S. *J. Org. Chem.* **2003**, *68*, 2903−2912.
(6) Berkessel, A.; Adrio, J. A.; Hüttenhain, D.; Neudörfl, J. M. *J. Am. Chem. Soc.* **2006**, *128*, 8421−8426.
(7) Berkessel, A.; Adrio, J. A. *Adv. Synth. Catal.* **2004**, *346*, 275−280.

10.1021/ja0620181 CCC: $33.50

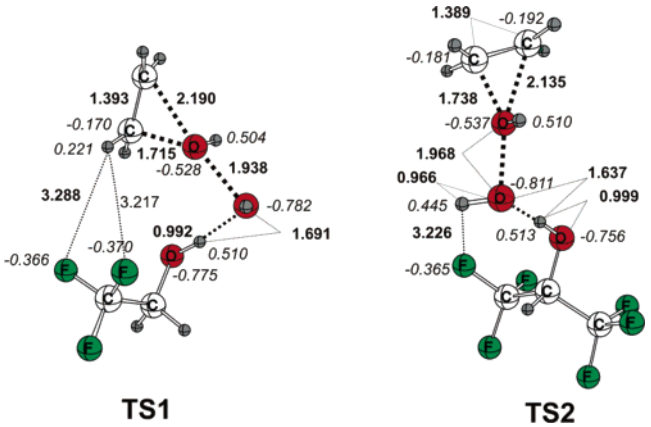

Figure 1. TSs of the TFE (**TS1**)- and HFIP (**TS2**)-catalyzed epoxidation of ethene by H_2O_2 as proposed by Shaik et al.[5] Bold numbers correspond to selected atom distances in Å; italic numbers correspond to natural atomic charges.

Scheme 1. Epoxidation of *Z*-Cyclooctene (**1**) by H_2O_2 in the Presence of HFIP

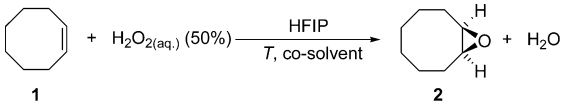

Table 1. Kinetic Rate Order with Respect to HFIP for the Epoxidation of *Z*-Cyclooctene (**1**) by Aqueous H_2O_2, as Determined with Four Different Cosolvents[6,7]

cosolvent	rate order in HFIP
$CHCl_3$	1.92 ± 0.09
$C_2H_4Cl_2$	2.78 ± 0.23
HFIPME[a]	2.72 ± 0.15
1,4-dioxane	3.0 ± 0.7

[a] 1,1,1,3,3,3-Hexafluoro-2-propyl methyl ether.

literature,[4,8] only little attention had been paid to the experimental elucidation of the mechanism of this process. We have recently presented a thorough kinetic analysis of the epoxidation of *Z*-cyclooctene (**1**) by aqueous H_2O_2 in HFIP as solvent (Scheme 1).[6] We were able to demonstrate that the reaction kinetics follow a first-order dependence with respect to the olefinic substrate as well the oxidant, suggesting a monomolecular participation of these components in the rate-determining step. On the other hand, a rate order of 2−3 with respect to the concentration of the fluorinated alcohol solvent is observed for several cosolvents (Table 1).[9]

To determine the activation parameters $\Delta H^{\ddagger}$ and $\Delta S^{\ddagger}$, the epoxidation of **1** (Scheme 1) was performed in HFIP at six different temperatures between 30 and 55 °C. The resulting Eyring plot is shown in Figure 2. The large negative $\Delta S^{\ddagger}$ of −39 cal/mol·K points to a highly ordered TS of the rate-determining reaction step: typical $\Delta S^{\ddagger}$ values for olefin epoxidations by peracids range from −18 to −30 cal/mol·K.[10]

From the above kinetic results, we conclude (i) that two to three molecules of HFIP are involved in the rate-determining step of the kinetically dominant reaction path for oxygen transfer

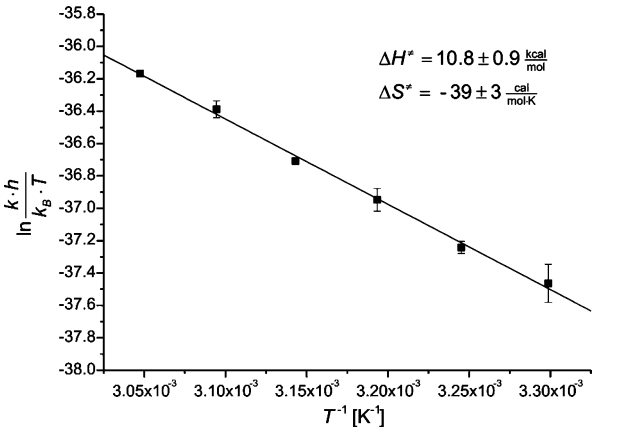

Figure 2. Eyring plot for the epoxidation of *Z*-cyclooctene (**1**) with H_2O_2 in HFIP at temperatures between 25 and 55 °C.

from H_2O_2 to the olefin and (ii) that the activation is brought about by highly ordered and therefore specific interactions, most likely through hydrogen bonding with the solvent molecules. A question results: Which spatial arrangement of H_2O_2, olefin, and fluorinated alcohol gives rise to the high reaction rates? We report herein the results of an extensive quantum-chemical search for configurationally and conformationally different transition states of the epoxidation involving hydrogen peroxide, ethylene or Z-butene as model substrate, and up to four molecules of HFIP.

Methods and Computational Details

Method Selection. DFT and especially Becke's three-parameter hybrid functional (B3)[11] combined with the Lee, Yang, and Parr (LYP)[12] correlation functional has gained increasing popularity for the calculation of molecular structure and energetics, in particular of organic reactions. In the controversy regarding the nature of oxygen-transfer processes in epoxidation reactions with peroxy acids or dioxiranes, DFT has proven its reliability for the description of these types of reactions.[13,14] The key process investigated in the work described in this article is oxygen transfer from hydrogen peroxide to an olefin. Oxygen-transfer processes from peroxides have proven dichotomous in that they may proceed via a concerted polar mechanism or by a stepwise biradical mechanism which involves O−O bond homolysis.[5,15−19] Experimentally,[15] and in particular theoretically, these pathways are difficult to distinguish and to describe accurately. In the quantum-chemical analysis of dioxirane-mediated oxygen insertions into C−H bonds, the use of spin-restricted DFT (RDFT) suggested a concerted polar mechanism, whereas spin-unrestricted DFT (UDFT) predicted a stepwise mechanism with the formation of a biradical intermediate.[17−19] Furthermore, all concerted transition-state wavefunctions displayed an instability toward the spin-unrestricted solution.[18] Therefore, we

(8) Ravikumar, K. S.; Zhang, Y. M.; Bégué, J.-P.; Bonnet-Delpon, D. *Eur. J. Org. Chem.* **1998**, 2937−2940.
(9) Catalysis by Brønsted acid impurities can be excluded, as unstabilized hydrogen peroxide [aqueous solution, 50% (w/w); Aldrich (Catalog No. 51,681-3)] was utilized exclusively as oxidant. HFIP, *Z*-cyclooctene, and the cosolvents were freshly distilled from sodium carbonate.
(10) Dryuk, V. G. *Tetrahedron* **1976**, *32*, 2855−2866.
(11) Becke, A. D. *Phys. Rev. A* **1988**, *38*, 3098−3100. Becke, A. D. *J. Chem. Phys.* **1993**, *98*, 5648−5652.
(12) Lee, C.; Yang, W.; Parr, R. G. *Phys. Rev. B* **1988**, *37*, 785−789.
(13) Bach, R. D.; Dmitrenko, O. *J. Phys. Chem. A* **2003**, *107*, 4300−4306.
(14) Dmitrenko, O.; Bach, R. D. *J. Phys. Chem. A* **2004**, *108*, 6886−6892.
(15) Adam, W.; Curci, R.; D'Accolti, L.; Dinoi, A.; Fusco, C.; Gasparrini, F.; Kluge, R.; Paredes, R.; Schulz, M.; Smerz, A. K.; Veloza, L. A.; Weinkötz, S.; Winde, R. *Chem. Eur. J.* **1997**, *3*, 105−109. Gonzalez-Nunez, M. E.; Castellano, G.; Andreu, C.; Royo, J.; Baguena, M.; Mello, R.; Asensio, G. *J. Am. Chem. Soc.* **2001**, *123*, 7487−7491. Bravo, A.; Fontana, F.; Fronza, G.; Minisci, F.; Zhao, L. *J. Org. Chem.* **1998**, *63*, 254−263.
(16) Shustov, G. V.; Rauk, A. *J. Org. Chem.* **1998**, *63*, 5413−5422.
(17) Fokin, A. A.; Tkachenko, B. A.; Korshunov, O. I.; Gunchenko, P. A.; Schreiner, P. R. *J. Am. Chem. Soc.* **2001**, *123*, 11248−11252. Du, X.; Houk, K. N. *J. Org. Chem.* **1998**, *63*, 6480−6483.
(18) Freccero, M.; Gandolfi, R.; Sarzi-Amade, M.; Rastelli, A. *J. Org. Chem.* **2003**, *68*, 811−823.
(19) Glukhovtsev, M. N.; Canepa, C.; Bach, R. D. *J. Am. Chem. Soc.* **1998**, *120*, 10528−10533.

performed an additional stability check on all RDFT TSs and subjected them to a subsequent UDFT analysis.[5]

Our investigation includes a thermodynamic evaluation of hydrogen-bonded complexes consisting of up to four moieties of HFIP and H_2O_2. In these cases, a considerable portion of the binding energy is derived from dispersion, for which currently available density functionals cannot account.[20] Therefore, MP2 single-point calculations on optimized minimum DFT structures were applied in order to obtain an adequate estimate for this defect.[20] MP2 single-point calculations on DFT TSs were not considered further, as we have found the activation barrier for the reference reaction of oxygen transfer from H_2O_2 to ethene from an UMP2/UB3LYP approach ($\Delta E^{\ddagger} = 23.1$ kcal/mol) to differ significantly from the pure UDFT result ($\Delta E^{\ddagger} = 28.1$ kcal/mol) as well as the activation energy computed at the UCCSD(T)/UB3LYP level ($\Delta E^{\ddagger} = 27.0$ kcal/mol). This deviation (between UDFT and UMP2 activation barriers) can probably be attributed to the higher sensitivity of MP2 to the (in)stability of the reference wavefunction.

Computational Details. Simulations on model reactions were carried out using the hybrid B3LYP[11,12] functional and MP2 as implemented in the Gaussian03[21] suite of programs. Standard double- and triple-ζ split valence basis sets were utilized. Since hydrogen bonding plays a major role in the processes studied, particular attention was paid to the best possible quantum-chemical description of these interactions. Besides the incorporation of polarization functions for all elements, it was observed that, especially in DFT, basis set augmentation with diffuse functions is essential for adequate performance.[22] Therefore, geometry optimizations were generally performed with a 6-31+G(d,p) basis set. For the resulting structures, a refined single-point analysis with the more extensive 6-311++G(d,p) basis set was conducted.[23] To validate the adequacy of this approach, we also applied the larger 6-311++G(d,p) set of functions to the geometry optimization of a few small test structures. The resulting energies differed by less than 0.14 kcal/mol from the single-point energies of the B3LYP/6-31+G(d,p)-geometries. All stationary-point geometries presented were fully optimized and identified as minima or first-order saddle points on the potential energy surface by calculations of the vibrational frequencies. Computed harmonic vibrational frequencies, scaled by a factor of 0.964, were used to estimate zero-point energies and vibrational contributions to the enthalpy, entropy, and Gibbs free energy.[24] In the case of the smaller structures involving zero or one molecule of HFIP, the TSs were ascertained by following the intrinsic reaction coordinate (IRC).[25] Energies of molecular aggregates were corrected for the basis set superposition error (BSSE) using the counterpoise method of Boys and Bernardi.[26]

To assess the effects of nonspecific interactions of the optimized gas-phase ground- and transition-state structures with the surrounding solvent, we performed additional single-point evaluations in a polarized continuum model, making use of the integral equation formalism (IEFPCM).[21,27] As the model solvent for HFIP we chose acetone, as it has a dielectric constant most similar to that of HFIP ($\epsilon = 20.7$ for acetone; $\epsilon = 17.8$ for HFIP[28]) within the set of implemented solvents.

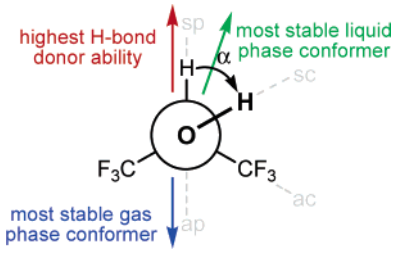

Figure 3. Dependence of the properties of monomeric HFIP on the conformation along the CO bond.

Unfortunately, the cavitation contribution to the free solvation energy is significantly overestimated, as HFIP is known to have an exceptionally low surface tension of 16.14 mN/m at 25 °C, as compared to that of acetone ($\gamma = 24.6$ mN/m).[29] Therefore, all cavitation contributions were reassigned on the basis of the concept of concave microscopic surface tension.[30,31]

Computational Results

The analysis of reaction pathways involving more than one molecule of fluorinated alcohol has to cope with high degrees of configurational and conformational flexibility. In an earlier study, we were able to show that the hydrogen bond donor ability of fluorinated alcohols, and in particular HFIP, is mainly dependent on two parameters: (i) the conformation of the alcohol monomer along the C−O bond and (ii) cooperative aggregation to H-bonded alcohol dimers and trimers.[6]

In the thermodynamically preferred gas-phase conformation, the HFIP monomer carries the hydroxyl group antiperiplanar (ap) to the adjacent CH. The two degenerate synclinal (sc) conformations are aproximately 1 kcal/mol less stable (Figure 3). This equilibrium is reversed if the alcohol is placed within a polarizable environment, as its absolute minimum structure now carries the OH sc or almost synperiplanar (sp) to the adjacent CH. On the basis of quantum-chemical considerations as well as single-crystal X-ray structures in which HFIP acts as a H-bond donor, we demonstrated that HFIP always takes on such a sc or even sp conformation when it is to act as a H-bond donor. In this conformation, the H-bond donor ability of HFIP is significantly increased.[6]

We were furthermore able to show that the H-bond donor ability of an HFIP hydroxyl group is greatly enhanced upon coordination of a second or even third molecule of HFIP.[6] Aggregation beyond the trimer has no significant additional effect.[6] Therefore, we constrained the current mechanistic investigation (i) to reaction pathways which involve HFIP in an sc or even sp conformation and (ii) to H-bonded HFIP aggregates comprising up to three alcohol monomers.

Catalysis by the HFIP Monomer. The polar concerted mechanism of electrophilic olefin epoxidation by H_2O_2, as proposed by Shaik,[5] proceeds via a nucleophilic attack of the olefinic double bond at the less negatively polarized oxygen atom of H_2O_2. In an S_N2-type fashion, the hydroxyl group is displaced. This formally leads to the formation of a protonated epoxide and a hydroxide anion. Subsequent proton transfer

(20) Cybulski, S. M.; Seversen, C. E. *J. Chem. Phys.* **2005**, *122*, 014117.
(21) Frisch, M. J.; et al. *Gaussian 03*, Revision C.02; Gaussian, Inc.: Wallingford, CT, 2004.
(22) Lynch, B. J.; Zhao, Y.; Truhlar, D. G. *J. Phys. Chem. A* **2003**, *107*, 1384−1388.
(23) Shaik et al. applied the 6-311++G(d, p) basis already in the geometry optimizations (see ref 5).
(24) The vibrational scaling factor (0.964 ± 0.023 for B3LYP/6-31+G(d,p)) used herein was obtained from the Computational Chemistry Comparison and Benchmark DataBase of the National Institute of Standards and Technology (http://srdata.nist.gov/cccbdb/). It comprises the comparison of 2585 computed and experimental vibrational frequencies of 265 molecules.
(25) Gonzalez, C.; Schlegel, H. B. *J. Chem. Phys.* **1989**, *90*, 2154−2161. Gonzalez, C.; Schlegel, H. B. *J. Phys. Chem.* **1990**, *94*, 5523−5527.
(26) Boys, S. F.; Bernardi, F. *Mol. Phys.* **1970**, *19*, 553−566.
(27) Cances, E.; Mennucci, B.; Tomasi, J. *J. Chem. Phys.* **1997**, *107*, 3032−3041. Cossi, M.; Barone, V.; Mennucci, B.; Tomasi, J. *Chem. Phys. Lett.* **1998**, *286*, 253−260. Mennucci, B.; Tomasi, J. *J. Chem. Phys.* **1997**, *106*, 5151−5158.
(28) Fioroni, M.; Burger, K.; Mark, A. E.; Roccatano, D. *J. Phys. Chem. B* **2001**, *105*, 10967−10975.
(29) http://www.dupont.com/polymerspecialties/HFIP_TechSheet.pdf, DuPont Chemical Solutions Enterprise.
(30) Sinanoglu, O. *J. Chem. Phys.* **1981**, *75*, 463−468.
(31) For details on the determination of the cavitation contribution to the free energy of solvation based on the concept of the concave microscopic surface tension, see the Supporting Information.

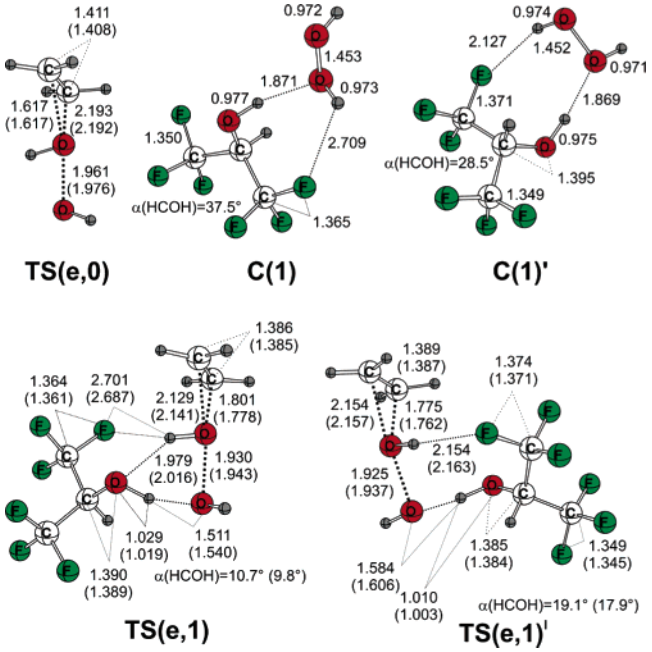

Figure 4. Stationary-point structures for the epoxidation of ethene with hydrogen peroxide in the absence and in the presence of one molecule of HFIP, optimized at RB3LYP/6-31+G(d,p) (selected bond lengths in Å; RB3LYP/6-311++G(d,p) results in parentheses).

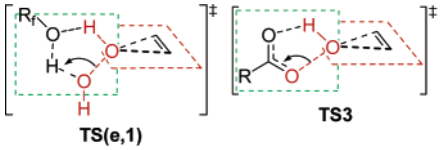

Figure 5. Spiro-bicyclic TSs in the electrophilic epoxidation of olefins: HFIP-assisted oxygen transfer from H_2O_2 to ethene via **TS(e,1)** (left) and percarboxylic acid-mediated epoxidation via **TS3** (right).

yields the epoxide and water. In all TSs presented by Shaik et al. (Figure 1), the most positively charged position of the H_2O_2−olefin moiety, namely the proton of the nucleophilically attacked hydroxyl group (q_H = 0.504 e in **TS1** and 0.510 e in **TS2**), remains unguarded by any negatively charged part of the fluoroalcohols. We addressed the question of whether complementary contact of this proton with either a fluorine atom or even the oxygen atom of HFIP might stabilize the TS and faciliate the subsequent proton transfer and thus the epoxidation process itself. Indeed, two TSs (**TS(e,1)** and **TS(e,1)′**, Figure 4)[32] could be identified, both being lower in energy than **TS2** (Figure 1). The corresponding lowest energy aggregates of H_2O_2 and one molecule of HFIP are depicted as **C(1)** and **C(1)′** (Figure 4).

As anticipated, **TS(e,1)** and **TS(e,1)′** feature a noticeable interaction between the proton at the prospective epoxide oxygen atom and the fluoroalcohol oxygen atom (**TS(e,1)**) or the CF_3 group (**TS(e,1)′**). **TS(e,1)** has a spiro-bicyclic structure. The planes of the three-membered ring formed by the ethylene carbon atoms and the prospective epoxide oxygen atom and the five-membered ring formed by the three oxygen atoms and the connecting protons are perpendicular. This is in analogy to the "butterfly mechanism" of olefin epoxidation by percarboxylic acids via **TS3** (Figure 5).[13] IRC calculations demonstrate that, along this reaction path, a subsequent barrier-free, cascade-like proton transfer toward the formation of the epoxide and water takes place. A similar mode of activation was proposed earlier for the oxidation of thioxane by hydrogen peroxide in protic solvents.[33] In the non-protic 1,4-dioxane as solvent, a kinetic rate order of 2 with respect to H_2O_2 was observed and interpreted as a second molecule of oxidant acting as H-bond donor.

Twofold HFIP Activation. In the case of the twofold HFIP participation, two distinct motifs of activation could be identified

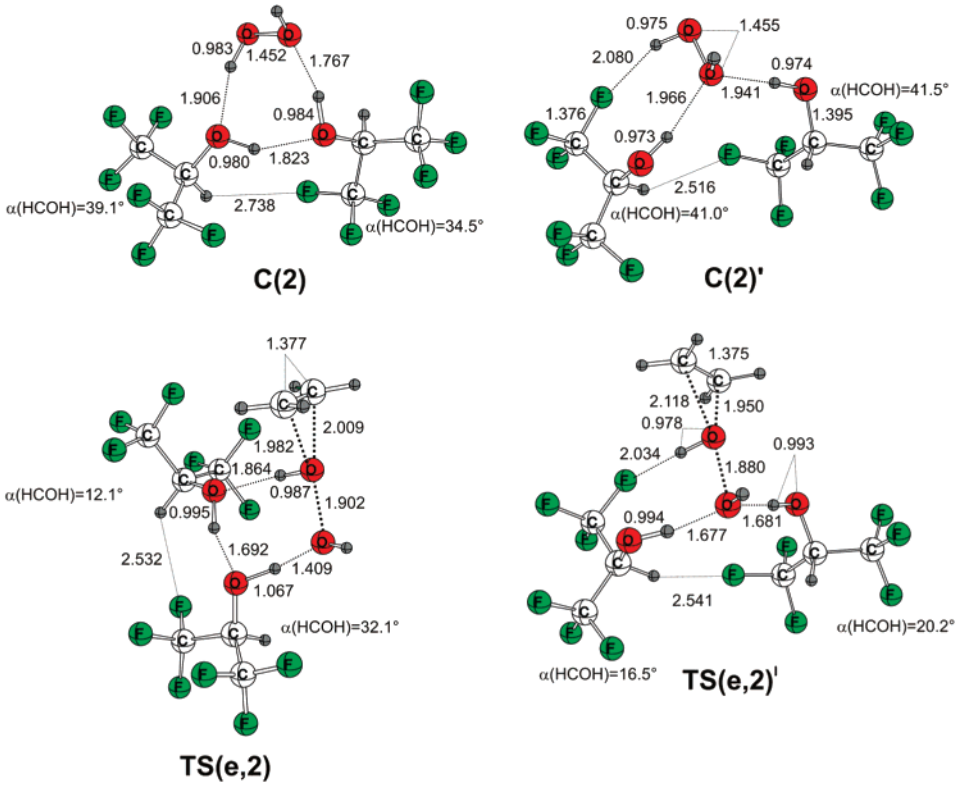

Figure 6. Stationary-point structures for the epoxidation of ethene with hydrogen peroxide in the presence of two molecules of HFIP, optimized at RB3LYP/6-31+G(d,p) (selected bond lengths in Å).

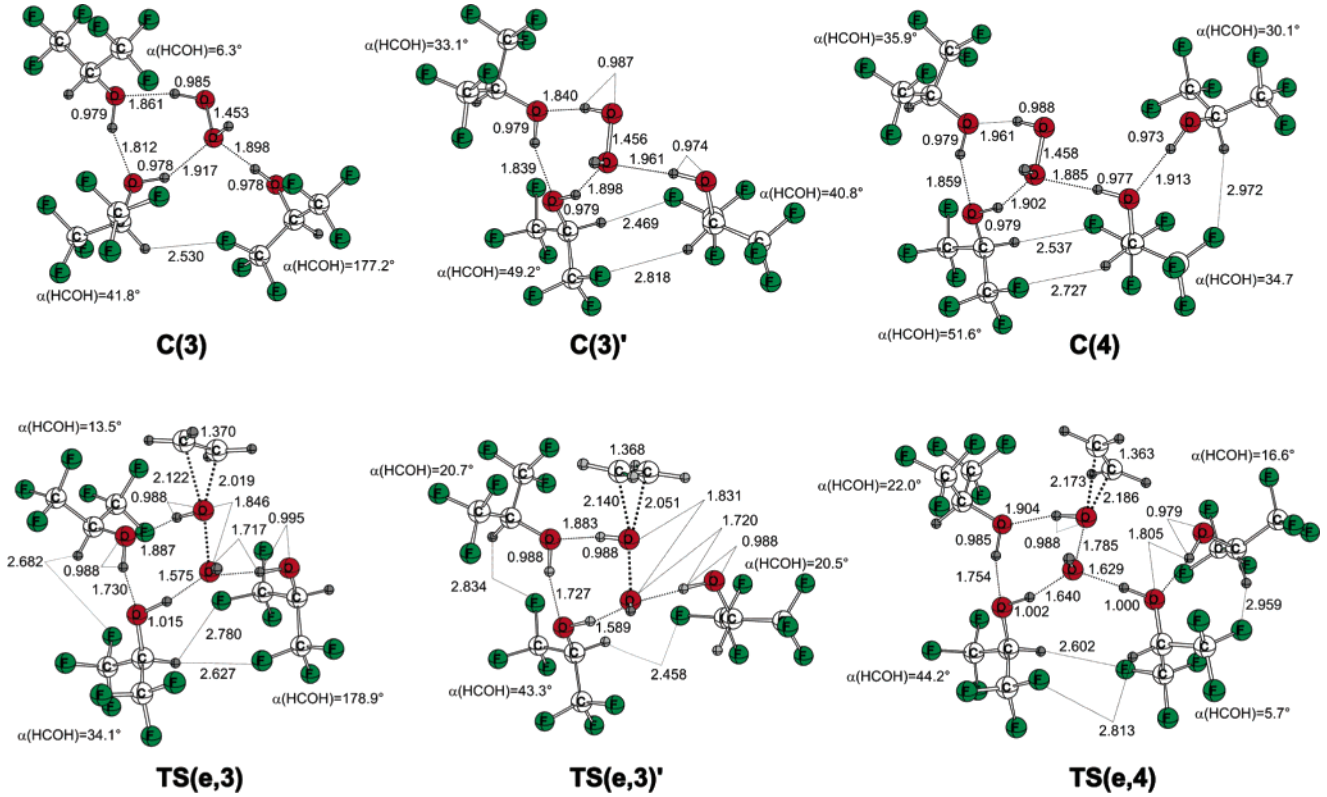

Figure 7. Stationary-point structures for the epoxidation of ethene with hydrogen peroxide in the presence of three and four molecules of HFIP, optimized at RB3LYP/6-31+G(d,p) (selected bond lengths in Å).

(Figure 6). (i) Both molecules of fluorinated alcohol act independently as hydrogen bond donors toward the oxidant (**TS-(e,2)′**). This results in high polarization of the hydrogen peroxide O−O bond and activation of the OH leaving group. (ii) Hydrogen peroxide is coordinated by the two alcoholic hydroxyl groups in a cyclic fashion, one HFIP acting as a hydrogen bond donor toward the leaving OH and the other one as a hydrogen bond acceptor toward the attacked hydroxyl group (**TS(e,2)**).

The internal hydrogen bond between the two fluorinated alcohols is expected to cooperatively increase the hydrogen bond donor ability of the alcohol molecule activating the leaving group.[6] Transition states for these reaction paths were found to be relatively close in energy (Figure 8, below). As reference ground-state structures, the 2:1 precomplexes of HFIP and H_2O_2, **C(2)** and **C(2)′**, were identified, containing the same hydrogen-bonding pattern as the transition states of the subsequent oxygen transfer (Figure 6).

Three- and Fourfold Activation. Even though the conformational freedom in aggregates of H_2O_2, ethene, and three or four molecules of HFIP is significantly increased, the number of reactive configurations which we were able to identify remains limited. The lowest energy transition states are depicted in Figure 7.

The hydrogen bond patterns leading to the most effective reduction of the activation barrier for oxygen transfer from H_2O_2 to ethene contain the cyclic element as in **TS(e,2)** of the twofold HFIP catalysis. Additionally, the OH leaving group is stabilized by accepting a second hydrogen bond from a third molecule of alcohol or a dimer of alcohols, respectively. Compared to these TSs, the structurally most similar precomplexes formed by three or four molecules of HFIP and one molecule of H_2O_2 were found in **C(3)**, **C(3)′**, and **C(4)**. **C(3)** and **TS(e,3)** are the only structures in this survey that contain a HFIP moiety as H-bond donor in an ap conformation.

Table 2. Comparison of Bond Length Parameters (in Å) for the Bonds Being Broken or Formed Via the Corresponding TS (All Geometries Optimized at RB3LYP/6-31+G(d,p))

transition structure	d(O−O)	d(C=C)	d(C_{olefin}−O)	Δd(C_{olefin}−O)
TS(e,0)	1.961	1.411	1.617; 2.193	0.576
TS(e,1)	1.930	1.386	1.801; 2.129	0.328
TS(e,1)′	1.925	1.389	1.775; 2.154	0.379
TS(e,2)	1.902	1.377	1.982; 2.009	0.027
TS(e,2)′	1.873	1.373	1.950; 2.118	0.168
TS(e,3)	1.846	1.370	2.019; 2.122	0.103
TS(e,3)′	1.831	1.368	2.051; 2.140	0.089
TS(e,4)	1.785	1.363	2.173; 2.186	0.013
TS(PFA)	1.852	1.369	2.054; 2.054	0

A close examination of the reaction pathways reveals that, as the order of HFIP activation increases, the transition state is shifted toward the substrates on the reaction coordinate. The O−O and C_{olefin}−C_{olefin} bond distances in the TS structures decrease whereas the average O−C_{olefin} bond distance increases with increasing order in HFIP activation (Table 2). Furthermore, there is a tendency toward a more symmetric approach of the electrophilic oxygen atom to the olefinic double bond. This is manifested by the difference in length of the two C−O bonds (Δd(C_{olefin}−O)) being formed in the TSs. The parameters of

(32) Ground-state cluster structures formed from HFIP and H_2O_2 and transition-state structures formed from HFIP, H_2O_2, and an olefin computed by us are generally denoted **C(*n*)** and **TS(o,*n*)**, where n (n = 0−4) refers to the number of HFIP molecules specifically coordinated to H_2O_2 and o indicates the olefin epoxidized in the corresponding TS (e = ethene; b = *Z*-butene). In the case of ground- and transition-state structures involving methanol instead of HFIP as the specifically coordinated solvent, the notation contains an additional m (**C(m,*n*)**, **TS(o,m,*n*)**).

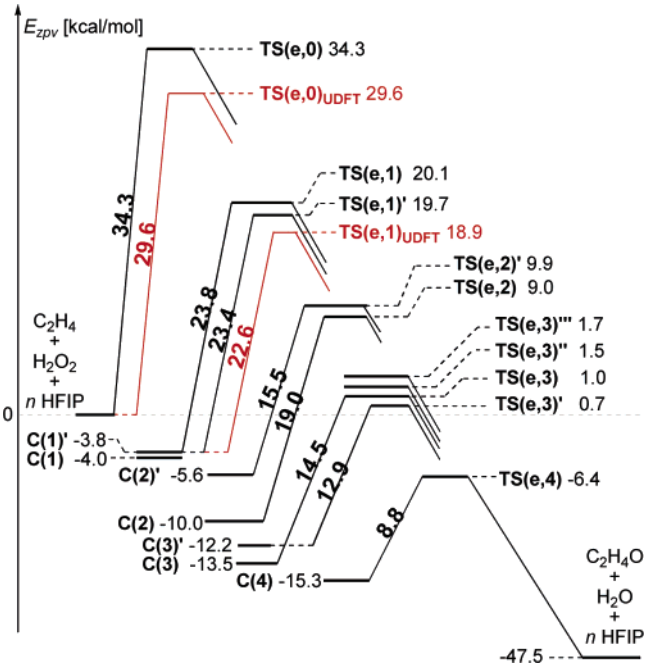

Figure 8. Energy profiles (gas phase) for the epoxidation of ethene in the presence of zero to four molecules of HFIP (ZPVE-corrected B3LYP/6-311++G(d,p)//B3LYP/6-31+G(d,p); RDFT results in black, UDFT results in red).

the bonds being formed or broken in **TS(e,3)** and **TS(e,3)′** approach those for the epoxidation of ethene by peroxyformic acid (**TS(PFA)**).[34]

An analysis of the H-bonding parameters shows that, in all cases where HFIP donates a hydrogen bond to the oxidant, this hydrogen bond is significantly contracted in the transition state, usually by more than 0.3 Å. The result of this significant contraction is the formation of a *low-barrier hydrogen bond*, characterized by an increase in covalency,[36] which effectively exerts the pronounced stabilization of the highly polar TSs through charge transfer. H-bonds between two HFIP molecules show the same trend, being regularly shortened by ca. 0.1 Å. This effect clearly indicates a cooperative H-bond enhancement. Additionally, we find a reduction of the $H_C COH$ dihedral angles in 14 of the 16 HFIP molecules within the seven presented reaction pathways. This result is in agreement with our earlier analysis of the H-bonding properties of HFIP, as the hydrogen bond donor ability is maximized toward the sp conformation of the alcohol.[6]

Gas-Phase Energetics. The gas-phase energetics for the described reaction pathways are sumarized in Figure 8. All reaction pathways are referenced to the isolated reactants. Complex formation was generally found to be exothermic. The average H-bonding interactions are between 2.8 and 4.0 kcal/mol per H-bond.

A comparison of the central barriers (**C(*n*)** + C_2H_4 → **TS-(e,*n*)**) in this series of reaction channels reveals a very

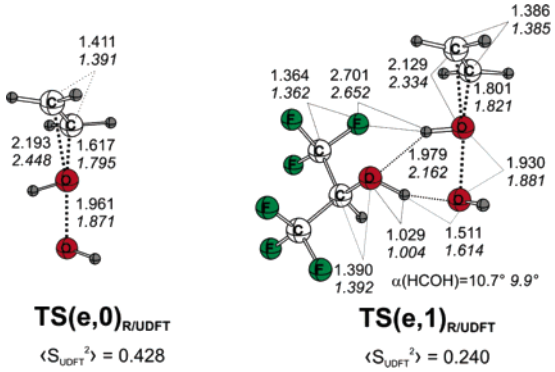

Figure 9. Comparison of transition-state structures for the epoxidation of ethene with hydrogen peroxide in the absence and in the presence of one molecule of HFIP, optimized at RB3LYP/6-31+G(d,p) and UB3LYP/6-31+G(d,p) (values in italics; all bond length parameters in Å).

pronounced decrease of the activation energy by up to ca. 75% with increasing degree of HFIP coordination. Specifically, the central activation barrier is reduced from 34.3 kcal/mol in the absence of HFIP to less than 9 kcal/mol upon coordination of four HFIP molecules.

Polar vs Diradical Mechanism. Much attention has been paid to the electronic nature of oxygen-transfer processes from peroxide species, as these processes have appeared to proceed either via a polar concerted or a diradical mechanism, depending on the quantum-chemical method by which they were analyzed.[16−18] Similar observations were made by Shaik[5] and coworkers in their initial theoretical analysis of the fluoroalcohol-assisted epoxidation with hydrogen peroxide. In all cases, they found competing pathways for concerted dipolar and stepwise mechanisms. All TS wavefunctions of the concerted mechanisms were unstable toward the unrestricted solutions. Considering this analysis in combination with experimental findings, the authors ruled out the stepwise pathways, even though they were mostly lower in energy and the concerted mechanism prevailed for only a very small fraction of all computed pathways. Therefore, a close inspection of the wavefunctions of the above pathways was conducted. As in the previous investigation by Shaik et al.,[5] we found the TS wavefunctions for HFIP-free and single-HFIP-activated pathways (**TS(e,0)**, **TS(e,1)**, **TS(e,1)′**, Figure 4) to contain an instability toward the spin-unrestricted solution, independent of the basis set used. Using an UB3LYP approach, transition states for a biradicaloid oxygen-transfer mechanism could be identified (**TS(e,0)$_{UDFT}$**, **TS(e,1)$_{UDFT}$**, Figure 9) which were lower in energy than the RDFT pathways ($\Delta\Delta E_{zpv}^{\ddagger}$(RDFT−UDFT) = −4.7 kcal/mol for **TS(e,0)$_{R/UDFT}$** and −0.8 kcal/mol for **TS(e,1)$_{R/UDFT}$**, Figure 8). In contrast, all wavefunctions of RDFT TSs involving a second, third, or fourth molecule of HFIP were *fully stable* toward the spin-unrestricted solution under the perturbations considered, and no corresponding UDFT pathway was found. We therefore conclude that, upon specific interaction with more than one molecule of HFIP, the reaction doubtlessly proceeds via a polar concerted pathway which—in contrast to the single-HFIP-assisted mechanism—unambiguously prevails over the diradical mechanism. This result is in perfect accord with the stereospecificity of the reaction.[5]

Solution-Phase Reaction. To determine the energetics of the reaction pathways in solution, the precomplexes **C(*n*)** as well as the transition states **TS(e,*n*)** were evaluated energetically

(33) Dankleff, M. A. P.; Curci, R.; Edwards, J. O.; Pyun, H.-Y. *J. Am. Chem. Soc.* **1968**, *90*, 3209−3218.
(34) For a structural comparison of TS(PFA) optimized herein at B3LYP/6-31+G(d,p) with a geometry optimized at B3LYP/6-31+G(d), see ref 35.
(35) Bach, R. D.; Glukhovtsev, M. N.; Gonzalez, C.; Marquez, M.; Estevez, C. M.; Baboul, A. G.; Schlegel, H. B. *J. Phys. Chem. A* **1997**, *101*, 6092−6100.
(36) Cleland, W. W.; Frey, P. A.; Gerlt, J. A. *J. Biol. Chem.* **1998**, *273*, 25529−25532.
(37) Specific values for the enthalpy and entropy of vaporization of HFIP and methanol are compiled in the Supporting Information.

Table 3. Thermodynamic Parameters for the Formation of HFIP−H_2O_2 Clusters from the Isolated Substances in Their Standard States at 298 K and 1 atm[a]

cluster formed	ΔH_f	$-T\Delta S_f$	ΔG_f
C(0)[b]	3.6 (3.8)[c]	−7.2	−3.5 (−3.4)[c]
C(1)	−1.6 (−1.5)[c]	−6.5	−8.2 (−8.0)[c]
C(2)	−2.2 (−3.4)[c]	−4.2	−6.4 (−7.6)[c]
C(3)′	−1.2 (−4.0)[c]	−3.3	−4.4 (−7.3)[c]
C(4)	−1.1 (−5.6)[c]	−3.1	−4.2 (−8.6)[c]

[a] BSSE-corrected B3LYP/6-311++G(d,p)//B3LYP/6-31+G(d,p). [b] Values correspond to uncoordinated H_2O_2 within a PCM. [c] Values correspond to BSSE-corrected MP2/6-31+G(2d,p)//B3LYP/6-31+G(d,p).

within a polarized continuum and referenced to the isolated components in their standard state at 298 K. This procedure involves three steps: (i) H_2O_2 and HFIP are transferred from the liquid into the gas phase. In this step, all intermolecular interactions are eliminated. The energy change of this process is accounted for by the enthalpy and entropy of vaporization.[37] (ii) The complexation of n HFIP ($n = 0-4$) and one H_2O_2 molecule is simulated quantum chemically, thus re-establishing the specific interactions within the complex **C(*n*)**. (iii) Formal transfer of these complexes from the gas phase into the PCM liquid phase covers the contributions of nonspecific interactions of these complexes with the surrounding solvent. Enthalpic and entropic contributions to the Gibbs free energy of solvation were separated on the basis of the assumption that the entropy is completely included in the entropy of cavitation, whereas all other solvation terms were attributed to the enthalpic contribution.[38] For the second and third steps, DFT was applied. In order to obtain a reasonable energetic picture of the reaction, the potential of each species in the liquid phase (μ_l) had to be adjusted with respect to the gas-phase potential (μ_g) according to the maximum possible concentration in which this species takes part in the reaction under our experimental conditions ($\mu_l = \mu_g + RT \ln[v_{gas}/v_l]$; [HFIP] = 9.47 mol/L; [$H_2O_2$] = 0.71 mol/L; [olefin] = 0.031 mol/L; [**C(*n*)**] = 0.71 mol/L; [**TS(*o*,*n*)**] = 0.031 mol/L).[39]

Table 3 shows the predicted equilibrium thermodynamics for the formation of the corresponding aggregates from the isolated substrates, with **C(0)** being "naked" H_2O_2 within the HFIP PCM. This evaluation served as the basis for the subsequent assignment of activation parameters to the various reaction channels. Only the structures lowest in energy are reported. As expected, an increasing entropic contribution, disfavoring larger cluster sizes, could be identified.

Figure 10 shows the overall dependence of the activation parameters on the number of HFIP molecules involved. Interestingly, the activation enthalpy of the epoxidation decreases steadily from zero to fourth order in HFIP. As expected, the activation entropy $-T\Delta S^{\ddagger}$ shows a continuous increase with increasing number of specifically coordinated HFIP molecules. Due to the increasing entropic contribution, the value of $\Delta G^{\ddagger}$ approaches "saturation" when three or four HFIP molecules are involved.

Methanol as Model Solvent. In analogy to the approach taken by Shaik et al.,[5] we tested our simulation of the reaction activation by HFIP against an equivalent simulation with methanol as the solvent. Again, the "naked" reaction in the absence of explicit methanol coordination, as well as stationary points of reaction pathways incorporating the explicit coordination of one, two, or three molecules of methanol, were geometrically optimized and energetically evaluated within a PCM (**C(m,*n*)**, **TS(m,e,*n*)**).

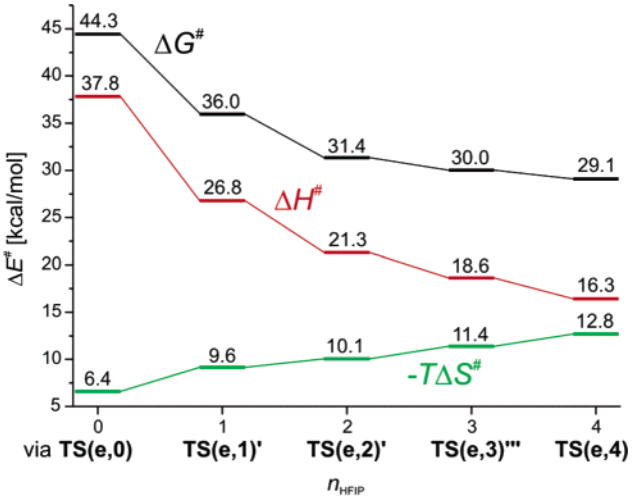

Figure 10. Activation parameters vs number of HFIP molecules for the epoxidation of ethene within a solution model at 298 K (RB3LYP/6-311++G(d,p)//RB3LYP/6-31+G(d,p)).

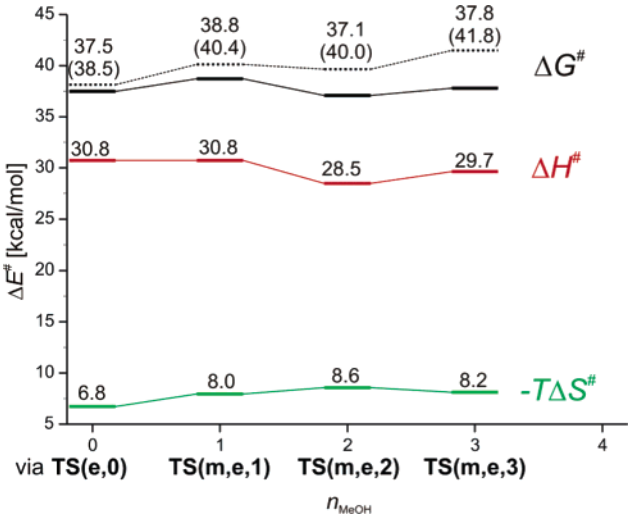

Figure 11. Activation parameters vs number of hydrogen-bonded methanol molecules for the epoxidation of ethene within a solution model for methanol at 298 K (RB3LYP/6-311++G(d,p)//RB3LYP/6-31+G(d,p)). Cavitation contributions in the PCM calculation of methanol were replaced according to the microscopic surface tension;[30] the dashed line refers to values in parentheses which result from unmodified IEFPCM calculations for methanol as implemented in Gaussian 03,[21] making use of the scaled particle approach for the evaluation of the cavitation contribution.

Embedding the "naked" reaction path in a PCM of methanol results in a more pronounced reduction of the activation barrier for ethene epoxidation as compared to inclusion in a HFIP PCM. This is in line with the highly polar nature of the oxygen-transfer process, which is more strongly stabilized by the more polar solvent (ϵ_r(MeOH) = 32.6; ϵ_r(HFIP) = 17.8). Intriguingly, however, we found no influence of explicit coordination of the solvent on the activation parameters of oxygen transfer (Figure 11). Therefore, the effect of a non-fluorinated alcohol such as methanol is solely to act as a polar reaction medium. In contrast to HFIP, specific hydrogen-bonding interaction with methanol is ineffective for reaction acceleration.

(38) Pais, A. A. C. C.; Sousa, A.; Eusebio, M. E.; Redinha, J. S. *Phys. Chem. Chem. Phys.* **2001**, *3*, 4001−4009.
(39) Ben-Naim, A. *J. Phys. Chem.* **1978**, *82*, 792−803.

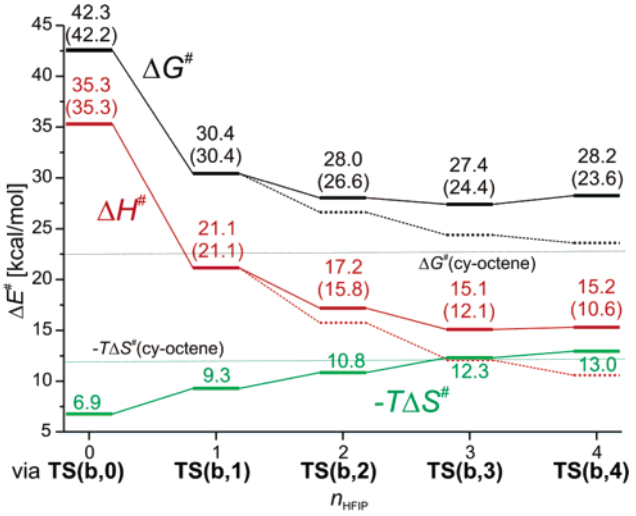

Figure 12. Activation parameters vs number of HFIP molecules for the epoxidation of *Z*-butene within a solution model at 298 K (RB3LYP/6-311++G(d,p)//RB3LYP/6-31+G(d,p)). Dashed lines refer to values in parentheses which include a correction for the dispersion interaction from a BSSE-corrected MP2/6-31+G(2d,p)//B3LYP/6-31+G(d,p) single-point calculation on the corresponding initial aggregates **C(*n*)**. $\Delta G^{\ddagger}$ (cy-octene) and $-T\Delta S^{\ddagger}$ (cy-octene) correspond to the experimentally determined activation parameters for the epoxidation of *Z*-cyclooctene at 298 K (Figure 2).

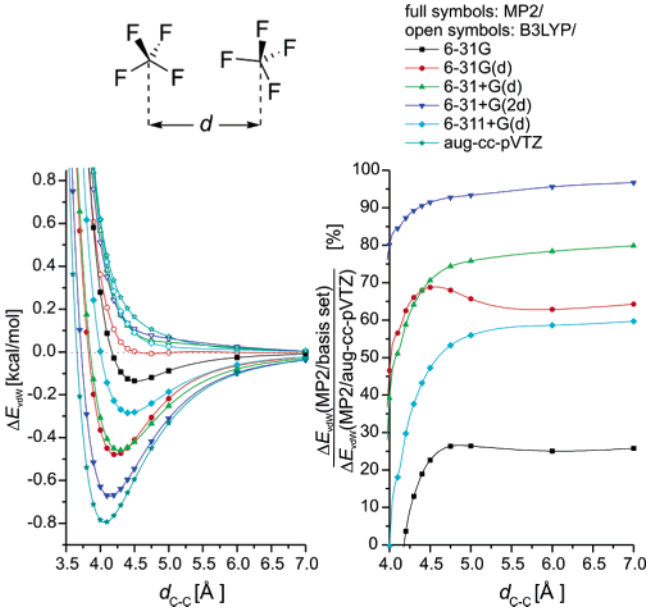

Figure 13. Basis set dependency of the van der Waals potential of the $(CF_4)_2$ dimer at DFT (B3LYP) and MP2 levels (left), and dispersion recovery at MP2 level with different split-valence basis sets compared to the extensive aug-cc-pVTZ basis (right).

***Z*-Butene as Model Substrate.** Our experimental study involved *Z*-cyclooctene (**1**). As the olefin closest to **1** in terms of epoxidation reactivity, but at a minimum computational cost, we chose *Z*-butene. Bach et al. calculated the epoxidation barrier of **1** with peroxyformic acid to be only ca. 0.6−0.9 kcal/mol lower than the corresponding barrier of *Z*-butene.[40] The general TS structure motifs were adopted from our initial computations on the model substrate ethene and subjected to a full optimization with *Z*-butene as the nucleophile. As in the previous investigation, the optimized gas-phase structures were evaluated energetically within a solvation model. The energetics as a function of the number of HFIP molecules are depicted in Figure 12. As expected, the entropic contribution to the Gibbs activation free energy has not changed significantly compared to the model for ethene epoxidation, whereas the activation enthalpy decreased for all pathways. The latter effect can be attributed to the higher nucleophilicity of the dialkyl-subtituted olefin. On the basis of the results that the activation entropy is not significantly affected by the nature of the olefin and that the enthalpic contribution is mainly governed by the nucleophilicity and therefore the substitution pattern of the olefin, we expect *Z*-butene to be an appropriate analogue of **1**. In contrast to the ethene epoxidation model, the enthalpic decrease in activation energy on going from a threefold to a fourfold HFIP activation vanishes in the corresponding model for *Z*-butene. This result can be attributed to steric repulsion between the large H_2O_2−HFIP aggregate and the bulkier olefin. Combined with the increasing entropic contribution, an overall increase in Gibbs free energy of activation is observed on going from a third- to a fourth-order HFIP participation. An absolute barrier minimum results at third order in HFIP (Figure 12). This is in remarkable accord with our experimentally determined rate order for the epoxidation of **1** (Table 1). Furthermore, the calculated activation entropy $-T\Delta S^{\ddagger}$ exceeds the experimental value by only 0.7 kcal/mol, which is within the experimental error margin. On the other hand, the calculated enthalpic value $\Delta H^{\ddagger} = 15.1$ kcal/mol deviates significantly from the experimental value of 10.8 kcal/mol. However, this deviation originates not from an inappropriate description of the oxygen-transfer process but from an inadequate treatment of the complexation thermodynamics due to the inability of DFT to account for dispersion interactions.[41] Most likely this causes a systematic underestimation of the stability of the higher-order aggregates relative to lower-order ones and therefore undervalues higher-order activation. To obtain a reasonable estimate of the missing interaction energy within the aggregates **C(*n*)** or **TS(b,*n*)**, we analyzed them by means of correlated ab initio methods, namely MP2 (vide infra).

Dispersion Contribution to Reaction Energetics. DFT is known to account for interaction energies from hydrogen bonding in good agreement with highly correlated ab initio methods.[42] Thus, we expected the major deficiency in the energetic evaluation of the aggregates **C(*n*)** or **TS(b,*n*)** to result from the missing dispersion interaction of the fluorinated alkyl groups. As demonstrated by Tsuzuki et al. for eight different $(CF_4)_2$ dimers, MP2 recovers most of the electron correlation, whereas the effects of electron correlation beyond MP2 are small.[43] We therefore restricted our investigation to the basis set dependency of the dispersion interaction. We monitored the potential of an arbitrarily chosen C_1-symmetric $(CF_4)_2$ dimer initially optimized at MP2/6-31+G(d,p) as a function of the C−C distance (Figure 13). Interaction energies were generally corrected for BSSE via the counterpoise algorithm.[26]

Indeed, the DFT potential is repulsive, independent of the basis set and the relative distance of the two fragments (Figure 13, left). In contrast, MP2 also accounts for a highly basis set dependent attractive dispersion interaction. For a subsequent

(40) Bach, R. D.; Dmitrenko, O.; Adam, W.; Schambony, S. *J. Am. Chem. Soc.* **2003**, *125*, 924−934.

(41) Tsuzuki, S.; Lüthi, H. P. *J. Chem. Phys.* **2001**, *114*, 3949−3957.

(42) Koch, W.; Holthausen, M. *A Chemist's Guide to Densitiy Functional Theory*; Wiley-VCH: Weinheim, 2001.

(43) Tsuzuki, S.; Uchimaru, T.; Mikami, M.; Urata, S. *J. Chem. Phys.* **2002**, *116*, 3309−3315.

single-point evaluation of the aggregates **C(*n*)** at the MP2 level, the 6-31+G(2d,p) basis proved to be the most economical choice, as it regularly recovers more than 90% of the dispersion compared to the extensive aug-cc-pVTZ basis at distances beyond 4.4 Å (Figure 13, right). Including solvation effects and BSSE corrections, we obtained a complexation energy for **C(1)** in good agreement with the DFT result ($\Delta\Delta H_f = 0.2$ kcal/mol). This result indeed indicates a reasonable treatment of the H-bonding interaction in DFT. On the other hand, for the higher-order aggregates, an increasing deviation between DFT and MP2 results was observed (Table 3). In the cases of **C(2)**, **C(3)′**, and **C(4)**, the differences amount to 1.2, 2.9, and 4.4 kcal/mol, respectively. Inclusion of these differences in the energetic evaluations of the corresponding DFT reaction paths—under the assumption that the magnitude of dispersion is about the same for **C(*n*)** and **TS(b,*n*)** at a given *n*—lowers the higher-order barriers significantly (Figure 12).[44] As a result of this additional correction, the higher-order pathways are even more favored over the path involving only one molecule of HFIP. For the third-order pathway, the activation enthalpy is now only 1.3 kcal above the experimental value for the epoxidation of *Z*-cyclooctene. Considering the slightly lower activation barrier for the peroxyformic acid-mediated epoxidation of *Z*-cyclooctene compared to *Z*-butene calculated by Bach et al.[40] ($\Delta\Delta E^{\ddagger} = 0.6-0.9$ kcal/mol), one can regard the simulated value to be within the experimental error margin. Furthermore, within an estimated error of 1−2 kcal/mol, the Gibbs free energy of activation approaches a saturation minimum at third order in HFIP, which is in agreement with the experimental finding.

Summary and Conclusion

In this article, we have presented a detailed mechanistic investigation of the epoxidation of olefins by hydrogen peroxide in the presence of 1,1,1,3,3,3-hexafluoro-2-propanol as solvent. The kinetic analysis revealed the reaction to be clearly first order in oxidant and olefin. With respect to the fluorinated alcohol, we found a kinetic rate order of 2−3. These results suggest that the rate-determining step of the reaction involves single molecules of olefin and H_2O_2, which is in line with an earlier quantum-chemical investigation by Shaik and co-workers.[5] With respect to the fluoroalcohol, we suggest two to three molecules of HFIP to be involved in the lowest energy reaction pathway(s).

We performed an extensive DFT simulation of configurationally and conformationally different reaction pathways involving one molecule of H_2O_2 and olefin and up to four molecules of HFIP. As model substrates, ethene and *Z*-butene were chosen. In their initial quantum-chemical investigation, Shaik and co-workers[5] proposed a reaction mechanism involving a single molecule of the fluorinated alcohol. Our simulations of ethene epoxidation revealed an additional reduction of the central gas-phase activation barrier by up to ca. 15 kcal/mol upon consideration of three additional molecules of HFIP. In contrast to the single HFIP TSs, we find the spin-restricted wavefunctions of the TSs with higher HFIP participation to be completely stable with respect to a spin-unrestricted solution. Furthermore, we do not find any competing pathways of a biradicaloid oxygen transfer with an UDFT approach. These findings not only demonstrate the higher reliability of the computed activation barriers with a single-reference wavefunction but also prove the dominance of the dipolar nature of the oxygen-transfer process in HFIP.

Embedding the simulated pathways in a solvation model led to a steady decrease of the activation enthalpy of ethene epoxidation with increasing number of specifically interacting HFIP molecules. As opposed to the activation enthalpy, an increasing entropic contribution was calculated with increasing order of HFIP participation. As a result, the Gibbs energy of activation approaches a saturation minimum. In contrast to the findings for HFIP, methanol as a non-fluorinated alcoholic solvent shows no influence of specific interaction, e.g., hydrogen bonding, on the reaction rate but provides a highly polar reaction field.

In a third set of DFT simulations, we chose *Z*-butene as a model substrate. Again, we found a similar trend of decreasing activation enthalpy and increasing activation entropy with increasing HFIP participation. Due to the steric demand of the bulkier *Z*-butene substrate, the Gibbs energy of activation for the epoxidation of *Z*-butene reaches an absolute minimum at third order in HFIP. This is in perfect agreement with the experimentally determined kinetic rate order for the epoxidation of *Z*-cyclooctene. Furthermore, the simulation also showed good correlation with the experimental value of the activation entropy. The activation enthalpy calculated at the DFT level differed significantly from the experimental value. We identified the inability of DFT to account for the increasingly important dispersion interaction between the fluorinated alkyl groups as a cause for this deviation. Incorporation of an electron correlation correction from MP2 single-point calculations on the DFT geometries of the H_2O_2−HFIP aggregates resulted in an additional stabilization of the higher-order reaction paths as compared to the single-HFIP-assisted mechanism. Under these conditions, activation enthalpies for the third- or fourth-order paths were found that are in excellent agreement with the experimental values.

Hydrogen bonding lies at the heart of many organocatalytic transformations.[45] Typically, catalysis is effected by single or double hydrogen bonds between the catalyst and the substrate(s). On the other hand, enzymatic catalysis in most cases involves multiple H-bond networks.[45] We believe that cooperative enhancement of hydrogen bond donation through multiple H-bond networks will be a new motif for the design of novel organocatalysts. Work in our laboratory aimed at the exploitation of the mechanistic information presented herein is currently underway.

Acknowledgment. This work was supported by the Regional Computing Centre Cologne (RRZK) and by the Fonds der Chemischen Industrie (Kekulé doctoral fellowship to J.A.A). This paper is dedicated to Prof. Dr. Dr. h.c. Lutz F. Tietze on the occasion of his upcoming 65th birthday.

Note Added after ASAP Publication. The third cosolvent in Table 1 was misidentified in the version of this paper published ASAP on September 22, 2006. The corrected version was published ASAP September 26, 2006.

Supporting Information Available: Experimental procedures, computational details, and the complete ref 21. This material is available free of charge via the Internet at http://pubs.acs.org.

JA0620181

(44) Transition-state energies of oxygen transfer were not recalculated using MP2 for reasons discussed in the section on Method Selection.

(45) Berkessel, A.; Gröger, H. *Asymmetric Organocatalysis*; Wiley-VCH: Weinheim, Germany, 2005. Taylor, M. S.; Jacobsen, E. N. *Angew. Chem., Int. Ed.* **2006**, *45*, 1520−1543.